Variation of nuclear level density with angular momentum

K. Banerjee, S. Bhattacharya, C. Bhattacharya, M. Gohil, S. Kundu, T. K. Rana, G. Mukherjee, R. Pandey, P. Roy, H. Pai, A. Dey, T. K. Ghosh, J. K. Meena, S. Mukhopadhyay, D. Pandit, S. Pal, and S. R. Banerjee
Variable Energy Cyclotron Centre, 1/AF Bidhan Nagar, Kolkata 700 064, India
(Received 5 February 2012; revised manuscript received 15 May 2012; published 11 June 2012)

Neutron evaporation energy spectra have been measured in coincidence with γ rays of different multiplicities for ^{119}Sb* in the excitation energy range of ~31–43 MeV. The inverse level density parameter (k) have been extracted for different angular momentum regions corresponding to different γ-ray multiplicities by comparing the experimental neutron energy spectra with statistical model prediction. It has been observed that the level density increases with the increase in angular momentum. Possible reasons for this variation have been discussed.

DOI: 10.1103/PhysRevC.85.064310 PACS number(s): 25.70.Jj, 25.70.Gh, 24.10.Pa

I. INTRODUCTION

Nuclear level density (NLD) is an important ingredient of the statistical model, which is generally used for studying a wide variety of nuclear reactions, such as particle evaporation, fission, multifragmentation, and spallation. An accurate determination of NLD, and its dependence on excitation energy and spin in particular, is essential for precise prediction of cross sections using the statistical models. For a spherical nucleus of mass number A at moderate excitation energy E^* and spin J, the single-particle level density, $\rho_{\rm int}(E^*, J)$, is calculated using the analytical expression based on Fermi gas model [1] as follows:

$$\rho_{\rm int}(E^*, J) = \frac{(2J+1)}{12}\left(\frac{\hbar^2}{2\Im_{\rm eff}}\right)^{3/2}\sqrt{a} \times \frac{\exp[2\sqrt{a(E^* - E_{\rm rot} - \Delta_P)}]}{(E^* - E_{\rm rot} - \Delta_P)^2}, \quad (1)$$

where a is the nuclear level density parameter, $E_{\rm rot}$ $[=\frac{\hbar^2}{2\Im_{\rm eff}}J(J+1)]$ is the rotational energy, and $\Im_{\rm eff}$ $[=\Im_0(1+\delta_1 J^2+\delta_2 J^4)]$ is the effective moment of inertia [2] of the system. The details of the parameters used in Eq. (1) are given in Table I.

For the nuclei with appreciable ground-state deformations, it has been conjectured by Ignatyuk *et al.* [3] that, at low excitation energies, there should be collective enhancement of NLD due to the coupling of the rotational as well as the vibrational degrees of freedom with the single-particle degrees of freedom, and the enhanced level density $\rho(E^*, J)$ may be expressed as

$$\rho(E^*, J) = \rho_{\rm int}(E^*, J)K_{\rm coll}(E^*), \quad (2)$$

where $K_{\rm coll}(E^*)$ $[=K_{\rm vib}(E^*)K_{\rm rot}(E^*)]$ is the collective enhancement factor, consisting of both vibrational and rotational contributions. In deformed nuclei, the most important contribution to the collective enhancement comes from the rotational excitations, whereas in the case of spherical nuclei, the collective enhancement can be caused by vibrational excitations [4]. The long-range correlations, which are mainly responsible for the enhancement of level density, are expected to die out at higher excitation. Björnholm, Bohr, and Mottleson [5] suggested that the collective enhancement should fade out beyond a critical temperature T_c, which is given by

$$T_c = \hbar\omega_0\beta_2 \sim 40A^{-1/3}\beta_2 \text{ MeV}, \quad (3)$$

where ω_0 is the mean oscillation frequency and β_2 is the ground-state nuclear quadrupole deformation parameter. However, the results of some of the recent experiments, although they indicate such changes in some cases, are not quite conclusive [6,7].

Although several attempts have been made in recent years to understand both theoretically as well as experimentally the excitation energy (temperature) dependence of NLD [8–11], the information available about its angular momentum dependence is quite limited. Henss *et al.* extracted the NLD at high spin by measuring the neutron spectra for the $1n$ evaporation channel in coincidence with the Yrast γ rays measured with a 4π gamma detector array [12], but they did not explore the dependence of NLD in different angular momentum regions. In a recent experiment, the γ-ray multiplicity-gated α-particle evaporation spectra were measured for a number of nuclei with $A \sim 110$ to 125 and excitation energies in the range of ~30 to 40 MeV [13]. In this measurement, the inverse level density parameter k ($k = A/\tilde{a}$) was found to increase with the increase in angular momentum, except for ^{113}Sb, where it showed a decreasing trend at higher J values. However, the calculations based on the statistical theory of hot rotating nuclei [14] predicted that the value of k would increase with J in all cases.

It is thus evident that the interplay of the key parameters, such as ground-state deformation, excitation energy, and spin in NLD has to be properly understood. The system chosen for the present study is ^{119}Sb, which is near the shell closure and has a ground-state deformation given by $\beta_2 = -0.122$ [15]. So, from Eq. (3), the collective enhancement of NLD due to this deformation, if any, is expected to be damped with the increase in excitation energy at $T_c = 0.99$ MeV. In the present paper, we report the measurement of γ-ray multiplicity-gated neutron energy spectra in the decay of ^{119}Sb* in the excitation energy range of ~31 to 43 MeV, which corresponds to the average temperature in the range of ~1.0 to 1.4 MeV. The light-ion–induced reaction (^{4}He + ^{115}In) has been chosen in the present study to populate the compound nucleus ^{119}Sb*, as it has some specific advantages over the heavy-ion fusion route of production, which is evident from Fig. 1. It is seen from the figure that, in the case of the light-ion–induced reaction (upper

TABLE I. Description of symbols used in Eq. (1).

Symbol	Meaning	Value
r_0	Radius parameter	1.17
$\delta 1$	Deformability coefficient	0.9×10^{-5}
$\delta 2$	Deformability coefficient	0.2×10^{-8}
ΔP	Pairing energy	$12/\sqrt{A}$
$\Im_0$	Rigid-body moment of inertia	$\frac{2}{5}A^{5/3}r_0^2$
E^*	Excitation energy	
$E_{\rm rot}$	Rotational energy	

part), there is only one major residue ^{117}Sb (yield >90%) produced via the $2n$ channel at $E^* = 31.3$ MeV; on the other hand, a similar compound nucleus (^{115}Sb*) at similar excitation energy produced through the heavy-ion fusion route, will lead to two prominent residues ^{113}Sb (yield ∼55%) and ^{113}Sn (yield ∼38%), produced via $2n$ and pn channels, respectively (lower part). So, the level density extracted in the latter case is not that of a particular nucleus; rather, it is averaged over the more-than-one nuclei (residues). As the excitation energy increases, more reaction channels open up; even then, at $E^* = 42.9$ MeV, the light-ion fusion route is still dominated by only the one residue ^{116}Sb (yield ∼77%), whereas the latter case is far worse because there are more than two dominant residues.

II. EXPERIMENTAL DETAILS

The experiment was carried out using ^{4}He ion beams at bombarding energies of 30 and 42 MeV from the Variable Energy Cyclotron Centre (VECC) cyclotron. A self-supporting ^{115}In target of thickness 1 mg/cm^2 was used. Four liquid scintillator (BC501A) detectors (typical dimensions ∼5″ × 5″ and 7″ × 5″) [16] were used to detect neutrons produced in this reaction in coincidence with a 50-element BaF_2-based low-energy γ multiplicity filter array [17] to estimate the populated angular momentum on an event-by-event basis. The filter was split into two blocks of 25 detectors each and was placed on the top and bottom of a thin-wall reaction chamber (wall thickness ∼3 mm) in a staggered castle-type geometry. The multiplicity filter was kept at 5 cm from the target position and typical solid angle coverage was ∼56%.

The neutron detectors were placed outside the scattering chamber at angles 75°, 90°, 105°, and 150° with respect to the beam direction and at a distance of 150 cm from the target. Neutron energies were measured using the time of flight (TOF) technique whereas the n-γ discrimination was achieved by pulse shape discrimination (PSD) and time of flight. To keep the background of the neutron detector at a minimum level, the beam dump was kept at 3 m away from the target and was well shielded with layers of lead and borated paraffin. The event collection was triggered when at least two of the multiplicity detectors fired in coincidence with any one of the neutron detectors. Empty frame run of nearly equal time duration was taken after each run to estimate the neutron background, which was subsequently used to correct the respective spectrum. The data were collected on an event-by-event basis using an online VME data acquisition system and were analyzed offline as detailed below.

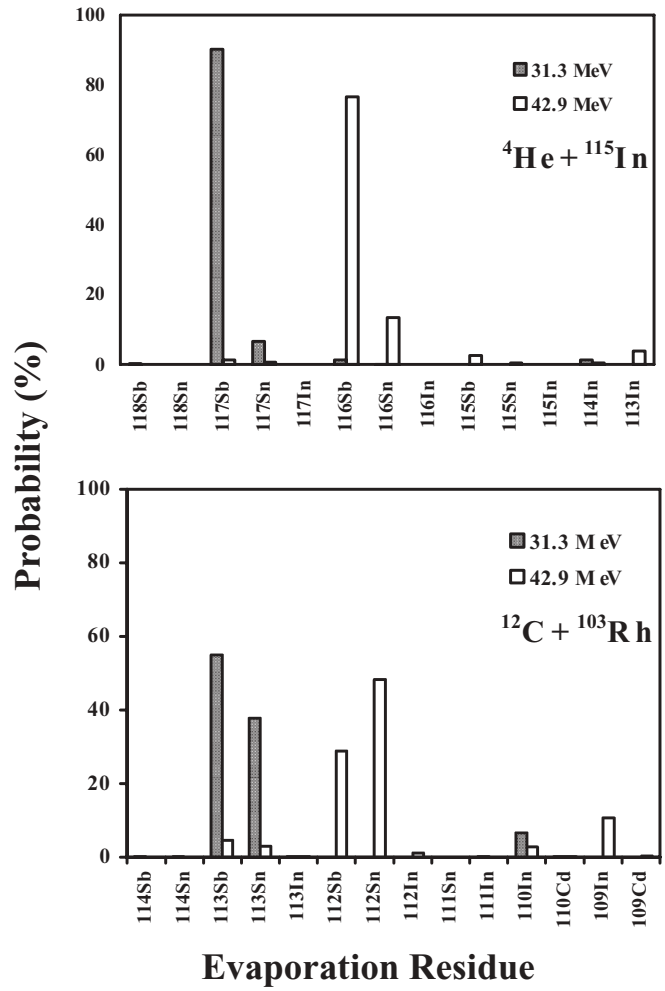

FIG. 1. Statistical model calculation of the relative yields of various evaporation residues produced in two different entrance channels.

III. DATA ANALYSIS

The measured γ-ray fold distribution was converted to an angular momentum distribution using the Monte Carlo simulation technique based on the GEANT3 toolkit [17]. Here, fold is defined as the number of BaF_2 detectors fired simultaneously in an event. The realistic experimental conditions (including the detector threshold and trigger condition) have been taken into account in the simulation. Different input multiplicities of the low-energy γ rays have been obtained by creating a random number according to the multiplicity distribution $P(M)$,

$$P(M) = \frac{(2M+1)}{1+\exp\left[\frac{(M-M_{\rm max})}{\delta m}\right]}, \quad (4)$$

where $M_{\rm max}$ is the maximum of the distribution and δm is the diffuseness. Low energy γ rays for each randomly generated multiplicity were thrown isotropically from the target center and the corresponding fold was recorded on an event-by-event basis. The angular momentum distribution used in the simulation was obtained from the statistical model code CASCADE [1]. The conversion of the angular momentum distribution to the multiplicity distribution was achieved using

TABLE II. Measured values of γ fold, average angular momentum, inverse level density parameter, and temperature.

Beam energy (MeV)	Fold	$\langle J \rangle$ ($\hbar$)	k (MeV)	T1 (MeV)	T2 (MeV)	T3 (MeV)
30	All	15.0 ± 5.9	8.6 ± 0.5	0.98 ± 0.03	0.53 ± 0.02	
30	2	12.6 ± 4.9	9.4 ± 0.2	1.05 ± 0.01	0.61 ± 0.01	
30	3	15.5 ± 5.2	8.7 ± 0.5	0.97 ± 0.03	0.52 ± 0.02	
30	4 and more	19.7 ± 6.2	8.0 ± 0.3	0.87 ± 0.02	0.38 ± 0.01	
42	All	16.9 ± 6.4	9.8 ± 0.2	1.39 ± 0.01	1.05 ± 0.01	0.39 ± 0.01
42	2	14.1 ± 5.2	11.1 ± 0.3	1.51 ± 0.02	1.16 ± 0.02	0.51 ± 0.01
42	3	16.8 ± 5.4	9.5 ± 0.5	1.36 ± 0.03	1.04 ± 0.03	0.39 ± 0.01
42	4 and more	21.1 ± 6.8	8.9 ± 0.3	1.26 ± 0.02	0.93 ± 0.02	0.12 ± 0.01

the relation $J = 2M + C$, where C is the free parameter which takes into account the angular momentum loss due to the particle evaporation and the emission of statistical γ rays. The measured fold distribution was then compared with the simulated fold distribution and the angular momentum distribution for different folds was extracted. The measured fold distribution (for 30 MeV incident energy) is displayed in Fig. 2(a) along with the corresponding GEANT3 simulation fit. The extracted angular momentum distributions corresponding to different folds of the multiplicity filter have also been plotted in Fig. 2(b). The extracted values of the average angular momenta $\langle J \rangle$ corresponding to different γ-ray folds of the multiplicity filter have been given in Table II.

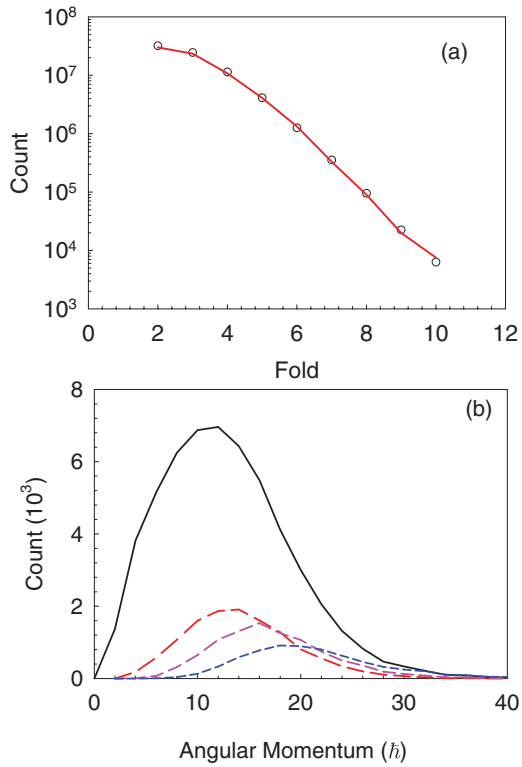

FIG. 2. (Color online) (a) Measured γ-ray fold spectrum for beam energy of 30 MeV (symbol, black) fit with GEANT3 simulation (solid line, red). (b) The solid (black) line indicates the incident angular momentum distribution used in the GEANT3 simulation. The long dashed (red), medium dash (pink), short dash (blue) lines are angular momentum distributions for fold 2, 3, and 4 & more, respectively.

Neutron time-of-flight data were converted to neutron energy using prompt gamma peaks in the TOF spectrum as a time reference. The efficiency correction for the neutron detector was done using the Monte Carlo computer code NEFF [18]. The laboratory neutron energy spectra were then corrected for background before further analysis. The experimental neutron energy spectra thus obtained at different laboratory angles have been shown in Fig. 3. We have also estimated the scattered neutron contribution due to scattering from the multiplicity filter by comparing the data from two runs: one with a full multiplicity filter and the other with only the lower part of the filter (25 detectors) in position. The contribution from scattered neutrons was found to be negligibly small.

The theoretical neutron energy spectrum was calculated using the statistical model code CASCADE by using the extracted angular momentum distributions for different folds as input (see Fig. 2). The phenomenological nuclear level density formula [Eq. (1)] was used in the calculation.

The NLD parameter "a" is related to the density of the single-particle levels near the Fermi surface and is influenced by the shell structure and shape of the nucleus, which in turn depend on excitation energy. An improved excitation-energy–dependent parametrization of the nuclear level density parameter has been proposed by Ignatyuk *et al.* [19], which incorporated the effect of nuclear shell structure at low excitation energy and goes smoothly to the liquid-drop value

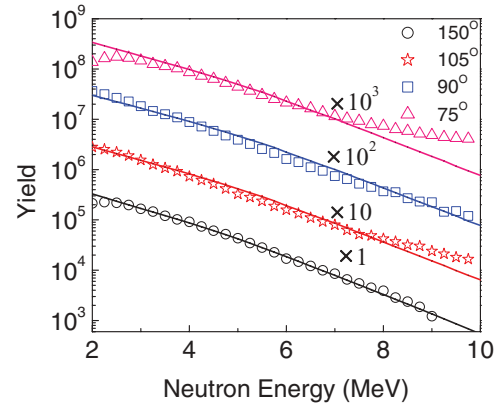

FIG. 3. (Color online) The experimental neutron energy spectra (symbol) at beam energy of 30 MeV for different angles displayed along with the respective statistical model calculations (solid lines).

expected at higher excitation energy. This is expressed as

$$a = \tilde{a}\left\{1 - \frac{\Delta S}{U}[1 - \exp(-\gamma U)]\right\}, \quad (5)$$

$$\gamma^{-1} = \frac{0.4A^{4/3}}{\tilde{a}}, \quad (6)$$

where $\tilde{a}$ is the asymptotic Fermi gas value of the liquid-drop NLD parameter at the excitation energy where shell effects are depleted leaving a smooth dependence on A. Here, ΔS is the shell correction obtained from the difference of the experimental and the liquid-drop model masses and γ is the rate at which the shell effect is depleted with the increase in excitation energy. The parameter k ($k = A/\tilde{a}$) has been tuned in the calculation to reproduce the experimental data. The transmission coefficients were calculated using the optical model, where the optical model parameters for neutron, proton, and alpha were taken from Refs. [20], [21], and [22], respectively. The calculated neutron energy spectrum in the c.m. frame thus obtained was converted to the laboratory frame using proper Jacobian transformation. The CASCADE spectra in the laboratory frame were then convoluted with the time-of-flight energy resolution as given by

$$\frac{\Delta E}{E} = 2\sqrt{\left(\frac{\Delta L}{L}\right)^2 + \left(\frac{\Delta t}{t}\right)^2}. \quad (7)$$

Here, ΔE is the energy resolution, ΔL is the uncertainty in flight path (detector length), Δt is the time resolution, and t is the flight time. Here, we have taken Δt as the transit time of the neutron within the detector. Organic scintillator detectors generally have time resolutions of the order of 1 ns, when measured using gamma source. However, in the case of neutron measurement the time response is mainly determined by the transit time of the neutron within the detector [23]. Transit time of neutron in the detector has been calculated using the NRESP7 code [18]. The convoluted spectra thus obtained were compared with the measured neutron energy spectra for different multiplicities using a χ^2 minimization technique to obtain the best fit.

For the extraction of inverse NLD parameter (k), we used the neutron data at the most backward angle (150°), where the contamination of the neutron spectrum by pre-equilibrium and other direct reaction processes are negligibly small. In the CASCADE calculation it was observed that the most sensitive parameter influencing the shape of the neutron spectra is the NLD parameter and the sensitivity is more for the higher-energy part of the spectra. The experimental neutron energy spectra at $\theta_{\rm lab} = 150^\circ$ for different γ-ray folds (inclusive, 2, 3, and 4 and more) for $E_{\rm lab} = 30$ and 42 MeV, together with the respective CASCADE predictions using the best-fit values of k, are presented in Figs. 4 and 5, respectively. The extracted values of the inverse level density parameters for different multiplicities are given in Table II. The k value thus obtained was used to calculate the neutron spectra at other angles, which has been shown in Fig. 3 along with the experimental spectra for comparison. The k value extracted from the neutron data at 150° is found to reproduce the data at 105° and 90° reasonably well. However, some deviation from the CASCADE calculation was observed for the higher-energy tail part of the neutron spectrum at 75°, which may be due to the contributions from other nonequilibrium processes.

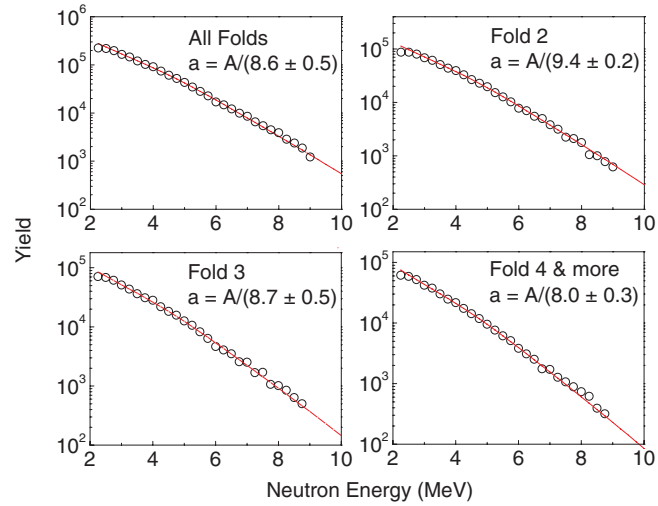

FIG. 4. (Color online) Experimental ($E_{\rm lab} = 30$ MeV) neutron energy spectra at $\theta_{\rm lab} = 150^\circ$ for different γ-ray folds (circles) displayed along with the respective CASCADE predictions (red solid lines).

IV. RESULTS AND DISCUSSIONS

The theoretical fits to the neutron energy spectra for different folds as shown in Figs. 4 and 5 indicate that the best-fit values of the level density parameter tend to increase at higher J values. For example, the value of a changes from $A/9.4$ (fold 2) to $A/8$ (fold 4 and more) for $E_{\rm lab} = 30$ MeV and from $A/11.1$ (fold 2) to $A/8.9$ (fold 4 and more) for $E_{\rm lab} = 42$ MeV. This indicates that there is some enhancement of level density in comparison with the same calculation using the standard form of CASCADE using identical spin distribution. The average temperatures corresponding to the measured neutron spectra were found to be ∼1 and 1.4 MeV for incident energies 30 and 42 MeV, respectively. In both the

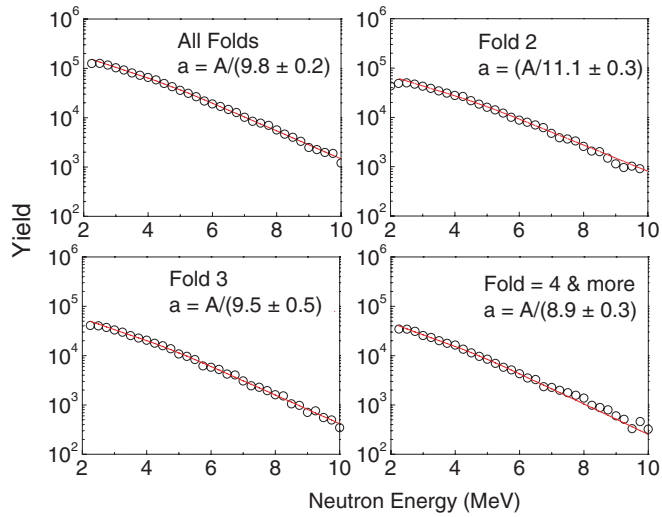

FIG. 5. (Color online) Same as Fig. 4 for $E_{\rm lab} = 42$ MeV.

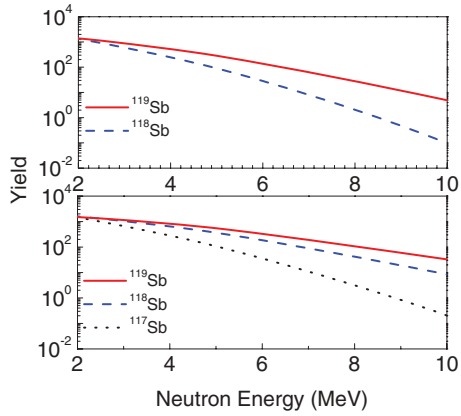

FIG. 6. (Color online) CASCADE-calculated neutron energy spectra from different stages of decay chain. Figure in the top for $E_{\rm lab} = 30$ MeV, in bottom for $E_{\rm lab} = 42$ MeV.

cases, the average temperatures are above T_c and therefore the collective enhancement due to the ground-state deformation is expected to be less significant.

In order to look into the above situation more deeply, we have investigated the characteristics of the neutrons emitted at intermediate stages. For this study, the present system comes in very handy as there is predominantly only one residue and that too is populated through a single path ($2n$ and $3n$ channels at $E_{\rm lab} = 30$ and 42 MeV, respectively). Figure 6 shows a typical statistical model calculation of the neutron energy spectra from the nuclei produced at various intermediate stages of the decay cascade. It is seen that the slopes (and temperatures) of the neutron energy spectra are different at different stages. The nuclear temperatures at different stages have been extracted and tabulated in Table II using the relation $U = aT^2$, where

$$U = E^* - E_{\rm rot} - S_n - \langle E_n \rangle. \quad (8)$$

The neutron separation energies (S_n) for ^{119}Sb, ^{118}Sb, and ^{117}Sb are 9.5, 7.4, and 9.8 MeV, respectively [24]. The average kinetic energies ($\langle E_n \rangle$) have been estimated from the respective energy spectra. For the present system, the critical temperature calculated using Eq. (3) is 0.99 MeV. It is clear from Table II that, for each fold, the temperature is above the critical temperature in the initial decay stages; however, during the final decay stage, it is well below the critical temperature. So the enhancement in level density visible in the present case may be, at least partially, due to the ground-state deformation.

V. SUMMARY AND CONCLUSION

The energy spectra of the neutrons emitted in the decay of ^{119}Sb* have been measured at backward angles in coincidence with the γ-ray multiplicity. The analysis of the γ-ray fold gated neutron energy spectrum reveals that the k value decreases with the increase in J, which is indicative of the fact that ρ increases with J. Detailed analysis of the neutron spectra from the intermediate stages of decay shows that the temperature during the final stage of decay chain is always much less than T_c. Thus, there is a finite possibility that the enhancement of NLD, or at least a part of it is due to the presence of ground-state deformation in the present case. Further systematic study in this direction is needed, however, to understand the variation in nuclear level density with angular momentum and also to elucidate the mechanism of enhancement of NLD observed in the present measurement.

ACKNOWLEDGMENTS

The authors are thankful to VECC Cyclotron operators for smooth running of the accelerator during the experiment.

[1] F. Puhlhofer, Nucl. Phys. A **280**, 267 (1976).
[2] S. Cohen, F. Plasil, and W. J. Swiatechi, Ann. Phys. (NY) **82**, 557 (1974).
[3] A. V. Ignatyuk, K. K. Istekov, and G. N. Smirenkin, Sov. J. Nucl. Phys. **29**, 450 (1979).
[4] R. J. Charity, Phys. Rev. C **82**, 014610 (2010).
[5] S. Björnholm, A. Bhor, and Mottelson, in *Proceedings of the International Conference on the Physics and Chemistry of Fission*, Rochester, New York, 1973 (IAEA, Vienna, 1974), Vol. 1, p. 367.
[6] A. R. Junghans, M. de Jong, H. G. Clerc, A. V. Ignatyuk, G. A. Kudyaev, and K. H. Schmidt, Nucl. Phys. A **629**, 635 (1998).
[7] S. Komarov, R. J. Charity, C. J. Chiara, W. Reviol, D. G. Sarantites, L. G. Sobotka, A. L. Caraley, M. P. Carpenter, and D. Seweryniak, Phys. Rev. C **75**, 064611 (2007).
[8] S. K. Kataria, V. S. Ramamurthy, and S. S. Kapoor, Phys. Rev. C **18**, 549 (1978).
[9] S. Shlomo and J. B. Natowitz, Phys. Rev. C **44**, 2878 (1991).
[10] S. Shlomo and J. B. Natowitz, Phys. Lett. B **252**, 187 (1990).
[11] R. J. Charity and L. G. Sobotka, Phys. Rev. C **71**, 024310 (2005).
[12] S. Henss *et al.*, Phys. Rev. Lett. **60**, 11 (1988).
[13] Y. K. Gupta, Bency John, D. C. Biswas, B. K. Nayak, A. Saxena, and R. K. Choudhury, Phys. Rev. C **78**, 054609 (2008).
[14] M. Aggarwal and S. Kailas, Phys. Rev. C **81**, 047302 (2010).
[15] P. Möller, J. R. Nix, W. D. Myers, and W. J. Swiatecki, At. Data Nucl. Data Tables **59**, 185 (1995).
[16] K. Banerjee, T. K. Ghosh, S. Kundu, T. K. Rana, C. Bhattacharya, J. K. Meena, G. Mukherjee, P. Mali, D. Gupta, S. Mukhopadhyay, D. Pandit, S. R. Banerjee, S. Bhattacharya, T. Bandopadhyay, and S. Chatterjee *et al.*, Nucl. Instr. Meth. A **608**, 440 (2009).
[17] Deepak Pandit, S. Mukhopadhyay, Srijit Bhattacharya, Surajit Pal, A. De, and S. R. Banerjee, Nucl. Instr. Meth. A **624**, 148 (2010).
[18] G. Dietze and H. Klein, PTB-ND-22 Report (1982).
[19] A. V. Ignatyuk, G. N. Smirenkin, and A. S. Tishin, Sov. J. Nucl. Phys. **21**, 255 (1975).
[20] D. Wilmore and P. E. Hodgson, Nucl. Phys. **55**, 673 (1964); P. E. Hodgson, Ann. Rev. Nucl. Sci. **17**, 1 (1967).
[21] F. G. Perey, Phys. Rev. **131**, 745 (1963).
[22] J. R. Huizenga and G. Igo, Nucl. Phys. **29**, 462 (1961).
[23] H. Klein and F. Brooks, POS (FNDA 2006), p. 97.
[24] [www.nndc.bnl.gov].